Decoding the role of triacylglycerol composition in the milk fat crystallisation behaviour: A study using buffalo milk fat fractions

LWT - Food Science and Technology 186 (2023) 115274

Contents lists available at ScienceDirect

LWT

journal homepage: www.elsevier.com/locate/lwt

Decoding the role of triacylglycerol composition in the milk fat crystallisation behaviour: A study using buffalo milk fat fractions

Yoga Pratama [a,b,*], Julia Seilert [c], Amin Sadeghpour [a], Elena Simone [d], Michael Rappolt [a,**]

[a] School of Food Science and Nutrition, Food Colloids and Bioprocessing Group, University of Leeds, Leeds, LS2 9JT, United Kingdom
[b] Department of Food Technology, Faculty of Animal and Agricultural Sciences, Diponegoro University, Semarang, 50275, Indonesia
[c] Department of Food Process Engineering, Technische Universität Berlin, Berlin, 10623, Germany
[d] Department of Applied Science and Technology, Politecnico di Torino, Torino, 10129, Italy

ARTICLE INFO

Keywords:
Milk fat
Buffalo milk
Crystallisation
Fractionation
Triacylglycerol

ABSTRACT

The role of triacylglycerols (TAGs) composition in milk fat crystallisation is evaluated from a new perspective by correlating the crystal structures and their predicted TAG contributors. Four different TAG groups, defined by their fatty acid (FA) chain length and saturation are proposed to explain the crystallisation behaviour of different milk fat samples, namely TAGs containing (i) fully saturated long chain FAs, (ii) single unsaturated long-chain FA and (iii) multi unsaturated long-chain FAs, as well as (iv) short-chain FAs. Samples containing different TAGs proportions were obtained from two-step dry fractionation of buffalo milk fat. Liquid chromatography and mass spectrometry (LCMS) was employed to determine the TAGs composition. The crystallisation characteristics were evaluated using small-angle X-ray scattering (SAXS), differential scanning calorimetry (DSC) and polarised light microscopy. The results confirm that fully saturated long chain TAGs are responsible for the formation of high melting point 2L-crystals (*d*-spacing: 44.1–49.7 Å), whilst the low melting point 3L-crystals (64.4–72.8 Å) are mainly contributed by long chain TAGs containing unsaturated fatty acids. Further, the crystallisation inhibiting effect of asymmetrical TAGs, containing short chain fatty acid (C4-6) is evident. As a final point, effects of the four TAG groups, each given with a specific composition, were examined closely also with respect to their influence on the nucleation and polymorphic transformation kinetics of milk fat crystals.

1. Introduction

Milk fat is one of the most important natural fats in the food industry. The annual processed milk fat (as butter and ghee) is estimated in around 12.5 million tonnes globally in 2020 (FAO, 2022). The milk fat is not only limited to manufacturing of dairy products such as butter, cheese and cream, but also widely used in confectionary like chocolate and candy. The presence of milk fat crystals in the food system affects their overall quality and textural properties, for example, in the stabilisation of whipped cream (Nguyen et al., 2015), the hardness of butter (Rønholt et al., 2013) and the bloom formation in confectionary products (Schmelzer & Hartel, 2001). However, the crystallisation behaviour of milk fat is still far from being fully understood. The main reason lies in its very large variety of triacylglycerols (TAGs), with more than 200 species amounting to >98% of total milk fat composition (Gresti et al., 1993; Jensen et al., 1991). Adding to this complexity, the composition of milk fat TAGs can greatly vary due to many factors such as milking species (Abd El-Salam & El-Shibiny, 2011; Gantner et al., 2015; Pratama et al., 2021; Smiddy et al., 2012), animal breed (Maurice-Van Eijndhoven et al., 2011; Soyeurt et al., 2006), type of feed (Grummer, 1991; Palmquist et al., 1993), season (Larsen et al., 2014; Romano et al., 2011; Tzompa-Sosa et al., 2018), and geographical factors (Shi et al., 2001). Milk fat also does not have any particular dominant TAG species as compared to other important fat commodities, such as cocoa butter and palm oil/fat. For instance, cocoa butter has three dominant triacylglycerols, namely POP, POS and SOS (note: P-palmitic, O-oleic, S-stearic) that account for about 80% of its total composition, which are the main drivers of crystallisation (Loisel et al., 1998). Whereas in palm oil, there are only two dominant TAGs, namely POP (28%) and POO (24%) (Omar et al., 2015).

* Corresponding author. School of Food Science and Nutrition, Food Colloids and Bioprocessing Group, University of Leeds, Leeds LS2 9JT, United Kingdom.
** Corresponding author.
E-mail addresses: fsyp@leeds.ac.uk, yogapratama@live.undip.ac.id (Y. Pratama), julia.seilert@tu-berlin.de (J. Seilert), A.Sadeghpour@leeds.ac.uk (A. Sadeghpour), elena.simone@polito.it (E. Simone), m.rappolt@leeds.ac.uk (M. Rappolt).

https://doi.org/10.1016/j.lwt.2023.115274
Received 5 May 2023; Received in revised form 6 September 2023; Accepted 7 September 2023
Available online 8 September 2023

Due to the complex TAGs composition, milk fat typically shows three broad endothermic peaks on differential scanning calorimetry (DSC) measurements (Grotenhuis et al., 1999; Tomaszewska-Gras, 2013). This led to the notion that milk fat consists of three separate TAG groups based on their melting point, which are commonly named high, medium and low melting fractions (HMF, MMF, LMF) (Deffense, 1993; Grotenhuis et al., 1999; Shi et al., 2001; Timms, 1980). Even though this interpretation is broadly accepted, there is no standardized definition for these three fractions, as the endothermic peak positions and relative areas are largely influenced by the thermal history of the sample before applying the heating scan. In fact, using different cooling rates can promote the formation of different fat polymorphs, with different melting points (Tomaszewska-Gras, 2013). Nonetheless, researchers have attempted to separate these fractions according to their melting ranges. Several fractionation techniques including dry and solvent methods with at least two steps of crystallisation have been put forward (Campos et al., 2003; Deffense, 1993; Romano et al., 2011; Timms, 1980).

In-situ combined DSC-SAXS studies have shown that the typical endothermic pattern is also influenced by polymorphic changes that might occur during DSC heating scans. The local minimum separating the first and second endothermic peak is actually influenced by an exothermic dip that corresponds to the polymorphic transformation from the α to β' polymorph (C. Lopez et al., 2001, 2005). Having pointed this out, it is more accurate to view the typical three endothermic peaks as superimposed events of (1) melting of the different TAG groups and (2) polymorphic transformations, including the melting of metastable structures and recrystallisation of more stable crystals followed by their subsequent final melting. Consequently, a quantification of the composition of different milk fat fractions using DSC alone cannot be accurate.

Having reviewed the existing studies on milk fat fractionation, many researchers focused on understanding and testing the different properties of each fraction, with the purpose of using them as ingredients for different food systems. Indeed, different physical properties, such as melting range, rheology and mechanical properties are a direct consequence of TAG compositional changes after fractionation. However, a more fundamental question needs to be addressed. That is, how varying TAGs composition affect the phase and crystallisation behaviour of milk fat. The effect of TAGs composition on polymorphism is crucial, as different polymorphs of the same compound may present very different physical properties; secondly, the TAGs composition can also affect the kinetics of crystallisation and polymorphic transformations. Both aspects are important for the design of manufacturing processes as well as for the stability of the final food material. As an example, a recent study (Christelle Lopez et al., 2006) showed that a one-step dry fractionation at 21 °C generated a high melting solid fraction with the tendency to crystallise into the β' phase, whereas the low melting liquid fraction remained in the α form, when a cooling rate −1 °C/min was applied.

Further attempts to elucidate the effect of varying milk fat TAGs composition on the physical properties of the resulting material have been carried out by mixing milk fat (H, M, L) melting fractions in different proportions and its effects to the phase behaviour (Marangoni & Lencki, 1998), the polymorphic transformations kinetics (Cisneros et al., 2006) and the formed microstructure (Ramel & Marangoni, 2016). It is worth mentioning that the effect of TAGs composition on the crystallisation behaviour of milk fat has also been demonstrated by our recent study. Cow and buffalo milk fat, which have different ratios of the HMF, MMF and LMF exhibited different kinetics in the formation of the β′ crystals at the slow cooling rate of −0.5 °C/min (Pratama et al., 2021). The buffalo milk fat, which has higher HMF and LMF proportion compared to cow milk fat, showed a slower β' formation.

Despite the wide literature on milk fat and milk fat fractions crystallisation, the concrete role of the TAGs composition in milk fat crystallisation remains unclear. We argue that using the HMF, MMF and LMF fractions and their ratios as sole argumentative basis for explaining the crystallisation behaviour of milk fat is not sufficient. This is supported by two reasons: (1) as abovementioned, there is no clear cut definition for these fractions and how to quantify them. Researchers have come up with different fractionation methods, which result in different TAGs composition; (2) fractionation cannot perfectly separate the different melting groups. For instance, TAGs that belong to the HMF (fully saturated TAGs) are also observed in the low melting fraction and *vice versa* (Christelle Lopez et al., 2006; Dimick et al., 1996; Van Aken et al., 1999). This inclusion is likely due to co-crystallisation during fractionation, which results in mixed crystals (Deffense, 1993), as well as the physical entrapment of low melting TAGs inside the crystalline network developed during crystallisation (Che Man et al., 1999).

With the limitations of the HMF, MMF and LMF framework to explain the milk fat crystallisation behaviour being put forward, we propose in the current study to elucidate the role of TAGs in milk fat crystallisation by grouping them by their molecular properties, such as chain length and saturation level. This approach is motivated by findings from previous studies (Christelle Lopez et al., 2006; Pratama et al., 2021, 2022) on the crystallisation of milk fat and how the different forming TAGs distribute in the existing polymorphs, depending on their molecular structure. It is possible to identify what TAGs are prevalent in a specific solid phase by determining not only their lattice spacing, but also their underlying electron density profile. Subsequently, this allows also to estimate the hydrocarbon chain tilt as well as the packing density – i.e., the area per chain – of the different polymorphs (Pratama et al., 2022).

The four different TAG groups, containing (i) fully saturated long chain FAs, (ii) single unsaturated long-chain FA and (iii) multi unsaturated long-chain FAs as well as (iv) short-chain FAs, have been identified as dominant types of TAGs in three different polymorphs and the molten TAG fraction, respectively. First, previous studies suggest that 2L-α crystals with lamellar stacking distance of about 47–48 Å are likely to be dominantly composed of fully saturated TAGs, such as PPP and PPS (Christelle Lopez et al., 2006; Pratama et al., 2021). Second, 3L-α crystals with *d*-spacing of 71–73 Å are predicted to be rich in TAGs containing both saturated and unsaturated fatty acids such as PMO and POO (note: M-myristic) (Pratama et al., 2021). Third, a 3L structure with *d*-spacing of 53–54 Å is composed mainly by asymmetrical TAGs containing short chain C4 to C6 fatty acids such as BuPS and BuPO (note: Bu-butyric) (Pratama et al., 2021). The presence of these types of TAGs is significant in milk fat, and their particular crystallisation behaviour has been reported (Pratama et al., 2022).

This 'chemical grouping' of TAGs approach is particularly suitable for dry fractioned buffalo milk fat. This type of milk fat has high quantities of fully saturated TAGs as well as short-chain fatty acids containing TAGs, when compared to cow milk fat (Pratama et al., 2021). Since all four groups are given in significant quantities, it is possible to separate them more effectively by fractionation, and in turn, allows a good evaluation of their role in milk fat crystallisation. Nevertheless, the presented experimental results are also relevant to other fat mixtures with similar TAGs composition (Pratama et al., 2021). To the best of our knowledge, this work is the first to report on the crystallisation behaviour TAGs mixtures obtained by dry fractionation of buffalo milk fat, and ultimately, will have an impact on the growing use of buffalo milk in industry, as it recently has become the second most produced milk globally (FAO, 2022). More importantly, the current approach's focus on TAG chemical structure, is universally applicable. For instance, it can be adapted in the endeavours to substitute milk fat with that of plant-based origin.

2. Materials and methods

2.1. Milk fat preparation and fractionation

Buffalo butter samples with fat content ≥82% in weight were purchased from La Marchesa (Terevola, Italy). Moisture and other milk solids were removed from butter by heat clarification, following the

method described in our previous work (Pratama et al., 2021). Briefly, 250 grams of butter were heated to 110 °C and kept at this temperature for 20 min at 100 rpm stirring with a magnetic stirrer (IKA RCT Basic, IKA-Werke GmbH & Co, Staufen, Germany). The coagulated milk solids were then vacuum filtered with a Buchner funnel and Whatman No. 1 filter paper. The resulting buffalo milk fat sample contains ≥99.5% fat content as confirmed by applying the Soxhlet extraction.

Milk fat fraction samples were obtained from two-step dry fractionation. In the first step, the milk fat sample was brought to melt at 70 °C for 15 min, before being transferred into a 100 ml jacketed cylinder connected to a Tamson TLC2 cooling circulator (PM Tamson Instruments, Bleiswijk, The Netherlands). Crystallisation was then conducted at 35 °C for 24 h, under 200 rpm stirring (IKA RW 11 Lab Egg overhead stirrer, IKA-Werke GmbH & Co, Staufen, Germany). The resulted slurry was then centrifuged at 10.000 RCF for 30 min at the corresponding crystallisation temperature (35 °C) in an Avanti J-30I centrifuge (Beckman Coulter, Indianapolis, United States). The liquid fraction was carefully separated using a pipette. In order to purify the solid from the residual liquid phase, the solid fraction in the centrifuge tube was washed with 5 ml petroleum ether (Alfa Aesar, Heysham, United Kingdom), followed by the same washing with 5 ml isobutanol (Fluorochem, Hadfield, United Kingdom), for three cycles in total(Yao et al., 2020). The tube was then left to dry for 24 h to remove the residual organic solvent. The solid fraction from the first crystallisation step is henceforth called the "Stearin" fraction. The second step fractionation used the liquid material pipetted from the first fractionation step. The same procedure for the first step was applied (i.e., melting, crystallisation, centrifugation and washing). The only difference was the crystallisation and centrifugation temperature, which was 25 °C. The resulting liquid fraction from the second step fractionation is henceforth referred as the "Olein" fraction, whereas the solid one is referred to as "Mid" fraction. Fractionation was conducted in three repeats. The terms Stearin, Mid and Olein fractions are used here to avoid confusion with high, medium, low melting fractions used in literature.

2.2. Yield calculation

To account for the loss of liquid during the washing step, the yield of fractionation was calculated using the solid fraction as the basis. For every fractionation step, the solid and liquid fraction yield (%) are calculated as below

$$Solid\ fraction\ (\%) = \frac{Solid\ weight}{Initial\ weight} \bullet 100 \quad \text{Eq. 1}$$

$$Liquid\ fraction\ (\%) = 100 - Solid\ fraction\ (\%) \quad \text{Eq. 2}$$

2.3. Liquid chromatography and mass spectrometry (LMCS) measurements

The TAGs composition of milk fat and milk fat fractions were evaluated according to the Zeb and Murkovich procedure (Zeb & Murkovic, 2010) in a Shimadzu LCMS 2020 (Japan) with a separation column Phenomenex Luna 3u C18(2) 100A LC Column 150 x 3.0 mm. The detailed procedure is described in our previous work (Pratama et al., 2021). Measurements were performed in triplicates and the collected data were processed in the LabSolutions software (version 5.97) to obtain chromatograms and mass spectra. Further chromatograms peak fittings, integration and plotting were carried out using OriginPro 2019b. Prior to fitting, the solvent contribution was removed. Peak fitting and integration followed the '*peak analyzer*' routine; briefly, the baseline was defined as a straight line from two ends each side of the peak and the position of the peaks were identified by the local maximum method. The total peak number and positions were cross referenced to the mass spectra obtained from the LabSolutions software. This allowed the exclusion of the unidentified peaks from the analysis.

2.4. X-ray scattering measurements and analysis

X-ray scattering measurements were conducted with a SAXSpace benchtop small and wide X-ray scattering instrument (Anton Paar GmbH, Graz, Austria). The wavelength, λ, was 0.154 nm, produced by a Cu-anode at 40 kV and 50 mA. The instrument is equipped with a TCstage 150 (Anton Paar GmbH, Graz, Austria) to provide a temperature controlled sample environment with accuracy ± 0.1 °C. The sample to detector distance (SDD) was 130 mm, which covers the small and wide angle regime with a q-range from 0.01 to 1.76 $Å^{-1}$ ($q = 4\pi \sin(\theta)/\lambda$). A Mythen micro-strip detector (Dectris Ltd, Baden, Switzerland) was used to record the 1D scattering patterns.

Samples of milk fat and its fractions were molten at >60 °C prior to filling (about 100 μL) into quartz capillary tubes (1.5 mm outside diameter), obtained from Capillary Tube Supplies Ltd. (Cornwall, United Kingdom). The capillaries were then sealed with wax. Measurements were carried out following three thermal procedures, where the samples were brought to melt at 60 °C for 10 min to erase the crystal memory and then cooled to −10 °C at three different rates (−5, −2, and −0.5 °C/min). At the end of the cooling scan, the samples were kept at constant temperature for 5 min before being heated back to 60 °C at a rate of 2 °C/min. Scattering patterns were collected every minute with a 30 s exposure time.

The SAXSTreat program was used to correct the position of the primary beam and the SAXSQuant program was employed to normalise the scattering pattern intensities by their transmission, and further used, to subtract the scattering contribution of the empty capillary. Both software packages are supplied by Anton Paar GmbH (Graz, Austria). Further data processing was carried out using OriginPro 2019b. This includes the further subtraction of the scattering contribution from the residual molten sample, peak fittings and plotting. In the case of multiple Bragg's peak per polymorph, the strongest peak was used to determine the crystallisation evolution.

2.5. Differential scanning calorimetry (DSC) measurements

Heat flow measurements were conducted using a DSC Q-20 (TA Instruments, Elstree-UK). About 15 mg of sample was placed in a sealed Tzero aluminium pan (TA Instruments, Elstree-UK) and subjected to three thermal procedures alike the ones for the X-ray measurements. Measurements were done in three repeats. Collected data were processed with the TA Instruments Universal Analysis software (Version 4.5A) and plotted in Origin Pro 2019b.

2.6. Polarised light microscopy (PLM) measurements

The microstructures of milk fat crystals were observed in a polarised light microscope (Leitz Dialux, Wetzlar, Germany). The lens was a Nikon M Plan 40x ELWD and the digital images were captured using a Canon EOS 7D Mark II (Canon, Japan) camera, providing a 5472 x 3072 pixels resolution. 50 μL of molten sample was placed in a Linkam CSS 450 hot stage (Linkam Instruments, Tadworth-UK), with the gap set at 100 μm. Two thermal procedures were used and the stage temperature was controlled with the Linksys 32 data capture programme (Linkam Instruments, Tadworth-UK). All samples were exposed to 60 °C for 10 min, in order to erase the crystal memory and then they were subjected to a cooling ramp of −5 °C/min down to 0 °C. The Stearin fraction was also slowly cooled at −0.5 °C/min after the same melting procedure. ImageJ 1.53a software (NIH, USA) was used for image processing. All captured images were scaled using a 1 mm graticule image, which was taken in the same microscopy set up. Image contrasts were enhanced for publication purpose.

2.7. Statistical analysis

One-way ANOVA were performed with the SPSS 28 software (IBM

Corp) for the subtotal of different TAGs groups (section 2.3). Significant differences ($p < 0.05$) comparing group means were determined, using Tukey post-hoc test.

3. Results and discussion

3.1. TAGs composition of milk fat fraction samples

The current dry fractionation procedure resulted in three fractions, i.e., the Stearin, Mid and Olein fractions with an extraction yield of 33.8 ± 3.7%, 23.6 ± 1.7% and 42.6 ± 2.9%, respectively. The two-step fractionation at 35 and 25 °C gave different results compared to the existing literature. Van Aken et al. (1999) reported the yield of Stearin fraction (>30 °C) to be 24% and the Olein fraction (<24 °C) to be 37%, leaving the Mid fraction (24-30 °C) portion to be 39%. Comparatively, the Stearin portion we found was bigger than estimated by Van Aken et al. (1999), even though the current fractionation was carried out at a higher crystallisation temperature (35 °C *vs* 30 °C in Van Aken et al. (1999)). On the other hand, the current Mid fraction yield is lower than in the previously reported study (Van Aken et al., 1999) albeit covering a broader temperature range of 25–35 °C. The Olein portion of both studies is nearly the same. It is worth noticing that the crystallisation temperatures are just slightly different (25 *vs* 24 °C), so the slightly lower Olein yield from Van Aken et al. (1999) might be comparable to the current result, if the experiments would have been both carried out at 25 °C. The major differences in yields most likely come from the fact that a different type of milk fat was used (current: buffalo, Van Aken et al. (1999): cow). We note that the difference in the milk fraction yield confirms our previous report (Pratama et al., 2021), which showed a higher percentage of high melting and low melting point TAGs in buffalo milk fat, when compared to cow milk fat. Whereas the middle melting point TAGs percentage is found to be lower in buffalo milk fat.

Table 1 shows the TAGs composition of the three different Stearin, Mid and Olein fractions and of the buffalo milk fat in total (henceforth, termed Whole Fat to differentiate it from the other fractions). 37 different TAG species have been successfully identified. Based on the different crystallisation behaviour of different types of TAGs (as mentioned earlier), we grouped these 37 TAGs into four categories, i.e., TAGs with (i) only saturated fatty acid (all-SFA), (ii) TAGs containing single unsaturated FA (single-UFA), (iii) TAGs containing multi unsaturated FA (multi-UFA) and (iv) short chain fatty acid ($N_C \leq 6$) containing TAGs (short-FA) to explain the effects of varying TAGs composition on milk fat crystallisation behaviour. The contribution of each group to the composition of each fraction is presented in Fig. 1, whereas chromatogram examples from highly different Stearin and Olein fractions are given in Fig. S1.

The Whole Fat consists of 55.8, 15.0, 9.5 and 9.6% w/w of short-FA, single-UFA, multi-UFA and all-SFA, respectively. All-SFA TAGs are present in decreasing order from 15.1 to 4.4% in the Stearin to Olein fractions ($p < 0.05$). This is expected because the all-SFA have higher melting points compared to the other TAGs; thus, they can be separated with high yield at higher fractionation temperature. On the other hand, the presence of unsaturation in the TAG molecules decreases the melting point significantly. As an example, the fully saturated PPP has a melting point of 63–67 °C, whilst the monounsaturated POP and polyunsaturated OPO melt at ranges of 33–35 °C and 19-21 °C, respectively (MacRidachis et al., 2021). Therefore, it is expected that the concentration of both single-UFA and multi-UFA groups should increase (as opposite to all-SFA), following the order of fractionation (Stearin < Mid < Olein). However, the current results show that there is no clear trend ($p > 0.05$) in single-UFA and multi-UFA concentration over the three fractions. The single-UFA were found in the range of 15–16% for all three fractions, whereas the multi-UFA were in a 9-10% range. A likely explanation for this is that single-UFA and multi-UFA co-crystallise and/or are entrapped in agglomerates of crystals during crystallisation, since unsaturated TAGs are equally present even at high crystallisation

Table 1
Triacylglycerol composition of milk fractions (shown as mean ± SD).

Compound	RT	Whole Fat	Stearin	Mid	Olein
Short chain FA-containing TAGs (short-FA)					
Bu-Co-P	2.87	1.57 ± 0.26	1.62 ± 0.59	1.29 ± 0.21	1.33 ± 0.09
Bu-C-M	3.30	1.08 ± 0.04	0.88 ± 0.05	0.94 ± 0.02	1.10 ± 0.03
Bu-C-P	3.73	1.92 ± 0.07	1.73 ± 0.07	2.04 ± 0.24	1.98 ± 0.04
Bu-La-P	4.33	1.74 ± 0.67	1.70 ± 0.17	2.53 ± 0.26	2.06 ± 0.01
Bu-La-O	4.57	1.19 ± 0.39	1.01 ± 0.39	1.79 ± 0.39	1.42 ± 0.10
Bu-M-P	5.20	5.67 ± 0.96	5.39 ± 0.88	5.01 ± 0.29	6.18 ± 0.11
Bu-M-O	5.30	3.50 ± 0.70	2.84 ± 0.74	3.53 ± 0.78	3.17 ± 0.49
Bu-P-L	5.47	3.83 ± 1.03	3.63 ± 0.23	3.38 ± 0.92	4.94 ± 0.43
Co-M-P	6.13	1.72 ± 0.41	1.88 ± 0.31	1.93 ± 0.32	2.51 ± 0.18
Bu-P-P	6.27	6.07 ± 0.44	5.11 ± 0.42	5.02 ± 0.55	6.17 ± 0.08
Bu-P-O	6.40	7.61 ± 0.60	6.82 ± 0.36	7.37 ± 0.45	7.79 ± 0.01
Bu-O-O	6.60	4.28 ± 0.28	3.24 ± 0.80	3.32 ± 0.30	5.34 ± 0.04
Co-P-P	7.37	3.25 ± 0.16	2.77 ± 0.36	2.74 ± 0.06	3.69 ± 0.04
Bu-P-S	7.60	5.79 ± 0.00	5.47 ± 0.64	5.58 ± 0.43	6.66 ± 0.45
Bu-S-O	7.83	4.16 ± 0.30	3.36 ± 0.58	3.65 ± 0.13	4.32 ± 0.04
Co-S-P	9.07	2.36 ± 0.08	2.07 ± 0.16	2.13 ± 0.14	2.49 ± 0.07
Sub Total		**55.8 ± 0.6^{b}**	**49.5 ± 0.7^{a}**	**52.3 ± 1.3^{a}**	**61.2 ± 0.8^{c}**
TAGs containing single unsaturated FA chain (single-UFA)					
P-Cy-O	9.37	2.60 ± 0.29	2.72 ± 0.58	2.61 ± 0.30	3.20 ± 0.63
P-La-O	13.93	1.83 ± 0.02	1.93 ± 0.27	1.79 ± 0.04	1.88 ± 0.00
P-M-L	14.43	1.08 ± 0.30	1.15 ± 0.36	1.16 ± 0.32	1.24 ± 0.18
P-M-O	17.50	2.93 ± 0.37	2.75 ± 0.15	3.06 ± 0.14	2.83 ± 0.06
O-P-P	22.00	3.65 ± 0.23	3.60 ± 0.46	3.90 ± 0.20	3.32 ± 0.24
S-P-O	27.83	2.30 ± 0.04	2.63 ± 0.19	2.69 ± 0.20	1.97 ± 0.04
S-S-O	35.27	0.66 ± 0.24	0.80 ± 0.23	0.82 ± 0.20	0.52 ± 0.01
Sub Total		**15.0 ± 0.7**	**15.6 ± 0.6**	**16.0 ± 0.6**	**15.0 ± 0.6**
TAGs containing multi unsaturated FA chains (multi-UFA)					
C-O-O	11.60	0.87 ± 0.14	1.15 ± 0.43	1.00 ± 0.36	0.74 ± 0.01
O-M-O	18.03	1.95 ± 0.04	1.86 ± 0.11	1.98 ± 0.20	2.07 ± 0.25
O-P-L	18.90	1.38 ± 0.64	1.59 ± 0.45	1.38 ± 0.09	0.97 ± 0.07
P-O-O	22.83	2.81 ± 0.30	3.17 ± 0.10	3.03 ± 0.15	3.22 ± 0.18
O-O-O	23.73	1.34 ± 0.27	1.21 ± 0.04	1.21 ± 0.08	1.28 ± 0.15
O-O-S	28.90	1.18 ± 0.29	1.29 ± 0.37	1.29 ± 0.29	1.08 ± 0.03
Sub Total		**9.5 ± 0.6**	**10.3 ± 0.9**	**9.9 ± 0.7**	**9.4 ± 0.6**
TAGs with long fully saturated FA (all-SFA)					
P-P-Cy	8.83	1.09 ± 0.05	1.03 ± 0.16	1.04 ± 0.09	1.24 ± 0.16
P-P-C	10.87	1.42 ± 0.09	1.39 ± 0.24	1.61 ± 0.05	1.16 ± 0.02

(*continued on next page*)

Table 1 (*continued*)

Compound	RT	Whole Fat	Stearin	Mid	Olein
La-P-P	13.43	1.41 ± 0.05	1.76 ± 0.08	2.04 ± 0.09	0.91 ± 0.02
M-P-P	16.80	1.82 ± 0.14	2.80 ± 0.08	2.79 ± 0.25	0.68 ± 0.00
P-P-P	21.13	1.76 ± 0.26	3.47 ± 0.24	2.32 ± 0.15	0.34 ± 0.05
P-P-S	26.80	1.34 ± 0.09	2.90 ± 0.36	1.36 ± 0.08	0.02 ± 0.02
S-P-S	33.97	0.78 ± 0.21	1.76 ± 0.41	0.71 ± 0.17	0.04 ± 0.04
Sub Total		**9.6 ± 0.4^{b}**	**15.1 ± 0.3^{d}**	**11.9 ± 0.1^{c}**	**4.4 ± 0.2^{a}**
Unidentified		10.1	9.5	9.9	10.1
Grand total		100	100	100	100

RT: retention-time; TAG: triacylglycerol; SD: standard deviation; Bu: butyric (C4), Co: caproic (C6), Cy: caprylic (C8), C: capric (C10), La: lauric (C12), M: myristic (C14), P: palmitic (C16), S: stearic (C18), O: oleic (C18:1), L: linoleic (C18:2) fatty acid. The different superscripts in the same row indicate statistical significant differences ($p < 005$).

temperatures.

The short-FAs instead show a clear increasing trend ($p < 0.05$) following the order of the fractionation, with the highest amount of this TAGs group contained in Olein (61.2%) and the lowest in Stearin (49.5%). This demonstrates the tendency of short-FA to remain in the liquid fraction, which implies a lower incorporation of this TAGs group into the solid crystals formed during fractionation. In our recent work, we hypothesized that that the TAGs containing unsaturated short-FA remain part of the liquid during crystallisation, due to their low nucleation point (Pratama et al., 2022). However, as 49.5% of short-FA coming from the whole milk fat remained were found in the Stearin fraction, a significant level of co-crystallisation and entrapment is clearly also taking place.

Having overviewed the composition of the four TAG groups in Fig. 1, it is apparent that the applied dry fractionation technique is not able to completely separate the TAGs according to their theoretical melting points or justify fully the so-called HMF-MMF-LMF fraction notation. Indeed all four TAG groups are still observed in the resulting fractions, only in different quantity. These results are beneficial for our approach to evaluate the effect of different types of TAGs on milk fat crystallisation.

3.2. Crystallisation behaviour of the different milk fat fractions

The small- and wide-angle X-ray scattering (SAXS and WAXS) patterns of the four milk fat samples with distinctly different TAG compositions are shown in Fig. 2. Applying three different cooling ramps, the plots show four different crystal structures at the end of the temperature profile (at −10 °C), i.e., α-2L (46–49.7 Å), β′-2L (44.1 Å), α-3L (72.8 Å), and β′-3L (64.4 Å) polymorphs, where values in the brackets indicate the *d*-spacings.

The α-2L crystals (peak at $q \cong 0.13$ Å^{-1}) shown with the highest intensity in the Stearin fraction and appeared at cooling rates of −5 and −2 °C/min. Whereas this polymorph was not visible in Olein at −2 and −0.5 °C/min, it was observed at the higher rate of −5 °C/min. Since the Stearin and Olein fractions contain all-SFA at the highest and the lowest level, respectively (Fig. 1), these results confirm that the α-2L crystals are more likely to form in the presence of all-SFA(Christelle Lopez et al., 2006; Pratama et al., 2021). It is worth noting that the *d*-spacing of the α-2L stacking varied among the samples. Stearin, Mid, Olein fractions and Whole Fat *d*-spacings were 49.7 Å, 48.3 Å, 46.0 Å and 48.0 Å, respectively. Because the crystals formed are made of different TAGs with similar chain length of the fatty acids (mixed crystal) (Breitschuh & Windhab, 1998), the resulting *d*-spacing is dictated by the proportion of such contributing TAGs. For instance, the Stearin fraction contains the highest amount of SPS, PPS and PPP (Table 2), which display a greater *d*-spacing compared to other all-SFA (e.g., LaPP and MPP), hence the Stearin fraction displays highest α-2L *d*-spacing. In contrast, Olein contains the lowest amount of those three TAGs, which results in a shorter *d*-spacing.

Another interesting result is the presence of the α-2L phase in the Olein fraction at high cooling rate of −5 °C/min, where the same crystal form is not observed at lower cooling rates. Certainly, the Olein fraction still contains a small amount of all-SFA (about 4%, Table 1). We speculate, that this little amount of TAGs needs higher undercooling for nucleation. Secondly, at higher undercooling conditions the clustering of all-SFA occurs at higher rate, inducing a partial segregation in the

Fig. 1. Distribution of four different TAG groups in milk fat and milk fat fraction samples. The different labels indicate statistically significant differences ($p < 0.05$).

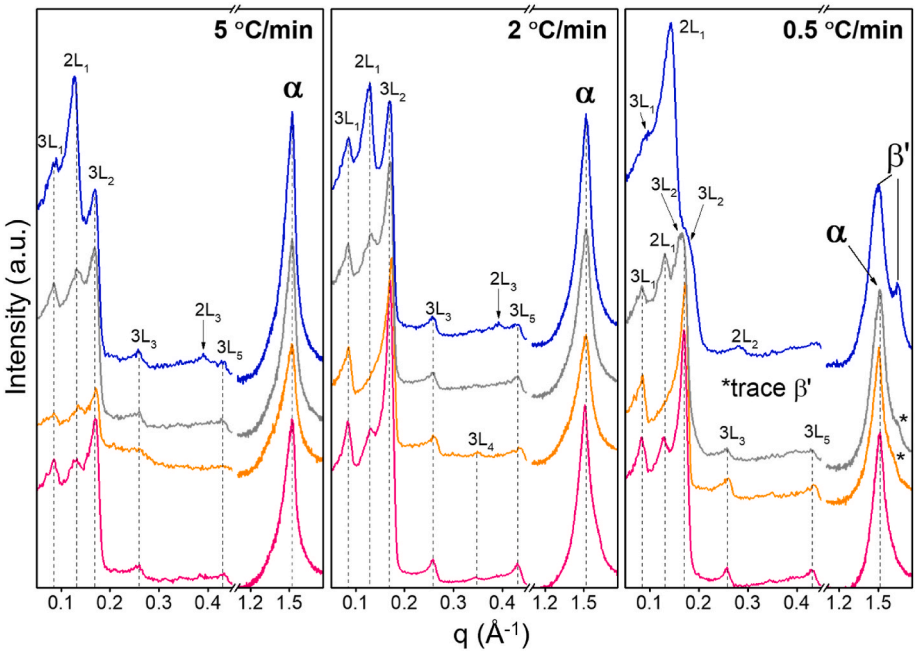

Fig. 2. X-ray scattering patterns of milk fat samples at −10 °C after cooling at different rates from melt. The patterns have been subtracted by its molten fat contributions to induce better clarity. The pattern of the Stearin fraction (blue line), the Mid fraction (gray line), the Olein fraction (orange line) and the Whole fat sample (pink line) are shown. (For interpretation of the references to colour in this figure legend, the reader is referred to the Web version of this article.)

Table 2
DSC thermogram events compilation.

Sample	Cooling rate (°C/min)	Cooling				Heating	
		α-2L	α-3L	β′-2L	β′-3L	β′-2L nucleation	Final melt
Whole Fat	5	18.7 ± 0.6	15.3 ± 0.5	-	-	13.5 ± 0.1	37.9 ± 0.4
	2	19.3 ± 0.5	13.9 ± 0.4	-	-	14.0 ± 0.1	37.8 ± 0.2
	0.5	25.0 ± 0.9	14.2 ± 0.4			13.7 ± 0.4	38.4 ± 0.3
Stearin	5	25.0 ± 0.4	13.6 ± 0.6	-	-	13.5 ± 0.5	43.5 ± 0.6
	2	25.6 ± 0.5	13.6 ± 0.7	-	-	13.1 ± 0.1	43.7 ± 0.5
	0.5	27.0 ± 0.2	-	24.0 ± 0.9	11.8 ± 0.4	21.0 ± 0.3[a]	44.3 ± 0.1
Mid	5	18.4 ± 1.0	13.3 ± 1.2	-	-	12.1 ± 0.6	37.8 ± 0.5
	2	19.1 ± 0.4	14.0 ± 0.6	-	-	12.8 ± 0.2	37.8 ± 0.5
	0.5	21.2 ± 0.7	14.5 ± 0.6	-	-	12.7 ± 0.3	38.9 ± 0.5
Olein	5	-	11.3 ± 0.5	-	-	-	17.1 ± 0.3
	2	-	11.5 ± 0.6	-	-	-	17.4 ± 0.7
	0.5	-	12.0 ± 0.9	-	-	-	17.1 ± 0.4

[a] melting of β′-3L.

mixture. This segregation allows the all-SFA to have a critical mass to form the α-2L crystal. On the other hand, the all-SFA are able to diffuse in the bulk of the sample at lower cooling rates and thus could not form this structure.

In contrast to the clear trend observed in the α-2L crystals, the α-3L structures (strongest 2nd order peak at $q = 0.17$ Å^{-1}) are shown in all samples at all cooling rates applied. We note, that the maximum intensity of this second order peak does not vary much among the different fractions, especially at −2 °C/min. Studies have shown that the α-3L phase nucleates at lower temperature than the α-2L phase (Christelle Lopez, 2018; Pratama et al., 2021), indicating that the crystals are most likely made of TAG groups with lower melting points. Therefore, the α-3L phase is expected to appear more abundantly in the reverse order of the fractionation temperature (i.e., Stearin < Mid < Olein). The current results, however, do not reflect this trend. This is consistent with relatively similar concentrations of single- and multi-UFA in all samples (Fig. 1). Thus, it is likely that the 3L architecture in milk fat is formed of TAGs containing at least one unsaturated fatty acid (Christelle Lopez et al., 2006; Pratama et al., 2021). The kinked fatty acid chain is likely to arrange in the monolayer regime of the lamellae; whereas, the bilayer contains predominantly the saturated chains (Pratama et al., 2021).

The present results prove the suitability of our 'chemical grouping' of TAGs approach, whilst at the same time giving evidence of the limitation of the HMF-MMF-LMF grouping for explaining the milk fat crystallisation behaviour. As mentioned above, the three melting fractions viewpoint is difficult to rationalize, simply because there is no clear categorization of which TAGs are included in each fraction. On top of that, it is hard to achieve a 'clean' fractionation of the different melting TAGs due to co-crystallisation and molecular entrapment.

Continuing with Fig. 2, a different result is obtained when the Stearin fraction is subjected to a slow cooling rate (−0.5 °C/min). In contrast to forming a α-polymorph, this particular fraction showed the formation of more stable β′ crystals, as indicated by its two characteristic diffraction peaks in the wide angle region ($q = 1.49$ and 1.64 Å^{-1}). Correspondingly, two lamellar architectures are observed in the small angle region, with *d*-spacing of 64.4 and 44.1 Å, which are attributed to β′-3L and β′-2L phases, respectively. Traces of the β′ phase can also be seen in the Mid and Olein fractions (subtle peak at $q = 1.64$ Å^{-1}). However, a strong peak at $q = 1.51$ Å^{-1} and the associated 2L and 3L peaks in the small angle regime indicate that most of the crystalline matter is in the α-polymorphs with hexagonal chain packing. These results confirm previous observations, where a higher Olein fraction content in milk fat delays the α → β′ polymorphic transformation (Christelle Lopez et al., 2006; Pratama et al., 2021). Further discussion on the kinetics will be addressed in the next section.

The crystal structure associated with asymmetric TAGs (containing short-FA) given by the β′-3L form with *d*-spacing around 53 Å, which was analysed in detail in our previous work (Pratama et al., 2022), was not observed in the current set of experiments. A possible explanation is that this polymorph has a relatively slow nucleation rate. Our previous experiments showed that this form is observable in buffalo milk fat after being frozen at ca. −18 °C for 3 weeks (Pratama et al., 2021). Whereas in cream and anhydrous milk fat, this structure is apparent after tempering at 4 °C for 60 h (Christelle Lopez, Bourgaux, Lesieur, & Ollivon, 2002). Therefore, it is not surprising that greater portions of short-FA remain liquid and accumulate also in the liquid Olein fraction during fractionation (Fig. 1).

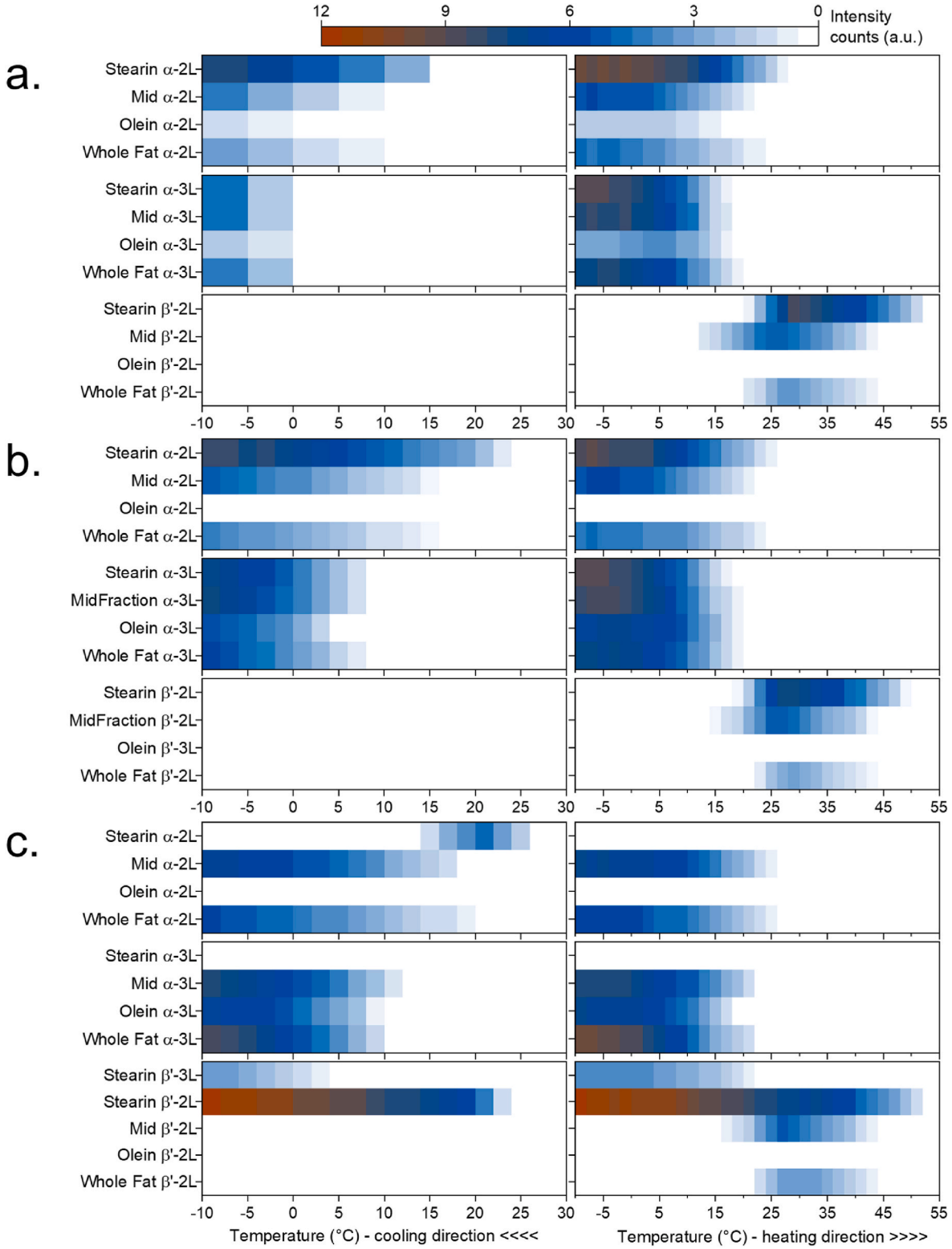

Fig. 3. Overview of crystal intensity evolution at different cooling rates: (a) −5, (b) −2 and (c) −0.5 °C/min which followed by subsequent heating at 2 °C/min.

3.3. Kinetics and evolution of crystal formation as affected by different TAG compositions

The phase evolution overview of all four milk fat samples and with the three different applied thermal procedures is presented in Fig. 3. All detailed X-ray intensity trends can be found in the supporting information Fig. S2 and **S3.** The twelve different experiments are further grouped based on three different characteristic crystallisation pathways observed. The first pathway (Fig. 4) shows a phase evolution, where only the α-polymorphs are observed during the cooling and heating ramps. This pattern is for instance observable in the Olein fraction at all the three different cooling rates (−5, −2 and −0.5 °C/min). Due to its low all-SFA content, the X-ray measurements confirm that the main crystalline form is in the 3L stacking architecture. This crystal structure nucleated during the cooling profile and subsequently melted upon heating without any polymorphic transformation. The thermogram (Fig. 4, bottom panels) agrees broadly with the X-ray observation as only one major exothermic (12.0 °C) and one endothermic (17.1 °C) peak are present during cooling and heating, respectively. However, an additional small exothermic event (12.5 °C) is observed in the DSC cooling regime, which can be associated with the nucleation of α-2L crystals. Correspondingly, a small endothermic peak (16 °C) was also observed during heating, which can be associated with the melting of the same crystal structure. Most likely, the all-SFA TAGs in the Olein fraction (about 4% as shown in Table 1) is responsible for these thermogram results. However, these additional subtle peaks were not captured in the SAXS measurements (Fig. 4, top panels). Differences in SAXS and DSC measurements can be explained considering the difference in the amount of sample used and the different sample holder geometry, which results in slightly different heat exchange efficiency albeit applying the same thermal procedure. It is worth noting that in general, the SAXS experiments reveal a thermal lag when compared to DSC measurements (i.e., displaying lower nucleation and higher melting points) due to a less efficient heat transfer of the SAXS setup (capillaries heated from both ends) compared to the DSC pans. For example, the onset of α-3L nucleation is shown at 9 and 12.0 °C for SAXS and DSC, respectively (Fig. 4).

The second pathway (Fig. 5) exhibits the formation of an α-polymorph during cooling and a polymorphic transformation from α to β' form upon subsequent heating. This crystallisation pathway is the most common among the three observed scenarios, and it was found in eight out of twelve experiments, i.e., Mid fraction and Whole Fat for all cooling rates, the Stearin fraction at −5 and −2 °C/min rate (Fig. 3, Figs. S2 and S3). The formation of α-phase upon cooling is indicated by two nucleation events, as observed on both SAXS and DSC measurements. The first, which occurs at higher temperature (between 18 and 25 °C depending on the cooling rate, Table 2), can be attributed to the formation of α-2L crystals, whereas the second nucleation event at lower temperature (13-15 °C, Table 2) is attributed to the appearance of α-3L crystals. It is worth noticing that the final amount of the crystals of each polymorphic form nucleated depended on the TAGs composition. For instance, Fig. 3b shows the Stearin fraction, which contains more all-SFA and has consequently more α-2L crystals at −10 °C, when compared to the Mid fraction that instead showed more of the α-3L crystals. Correspondingly, two main exothermic events are recorded in DSC, attributed to the α-2L (19.1 °C) and α-3L (14.0 °C) nucleation, respectively (Fig. 5, Table 2).

Upon heating, the Bragg peaks corresponding to the two α crystal structures showed a slight increase in intensity, followed by a decrease until their complete disappearance at 20-25 °C. The evolution of the amount of the α-2L form over time, is hard to quantify from the intensity of the main Bragg peak in the SAXS regime (q = 0.13 Å^{-1}), because it overlaps with a newly arising peak associated with the more stable β'-2L phase (q = 0.14 Å^{-1}, d-spacing = 44.1 Å), forming during heating at

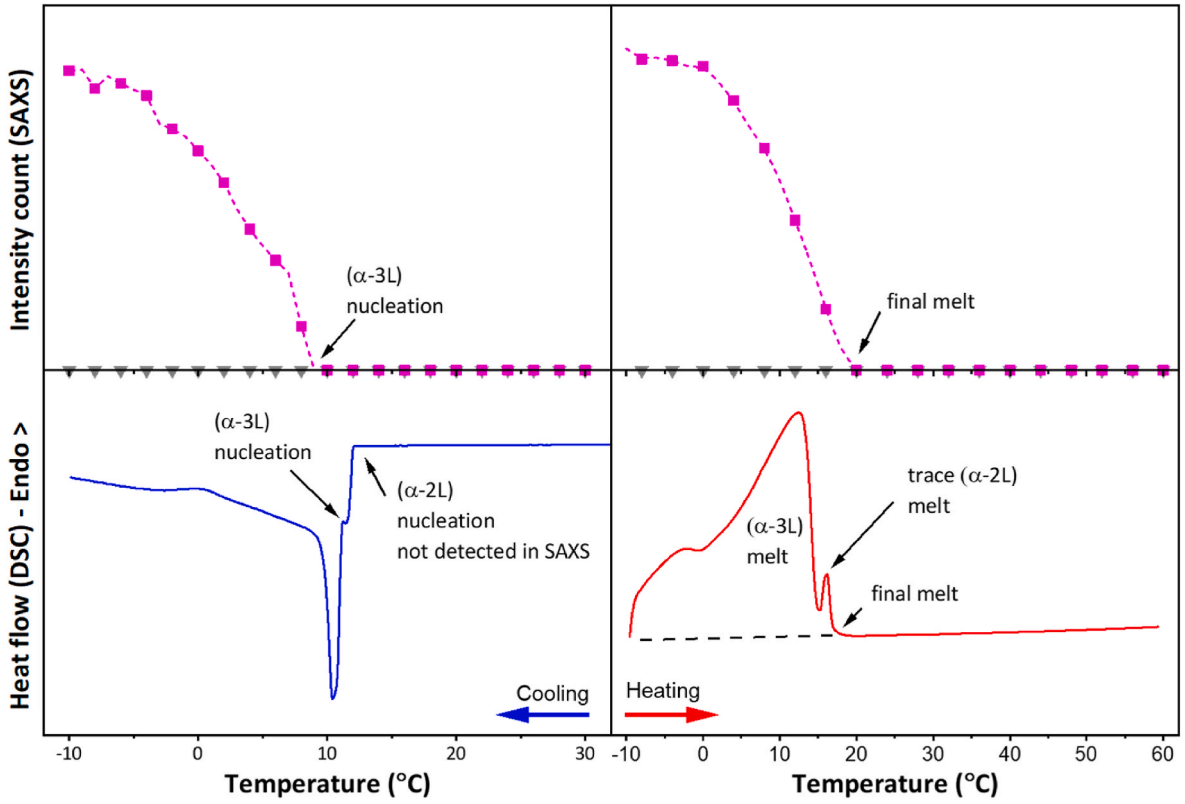

Fig. 4. Phase evolution pathway one: The β'-phase is absence on cooling and heating treatment. Shown result, Olein fraction cooled from melt at −0.5 °C/min to −10 °C, followed by subsequent heating at 2 °C/min to 60 °C. Trends of the α-2L phase (gray line with triangle symbols) are shown together with the α-3L phase (magenta line with square symbols).

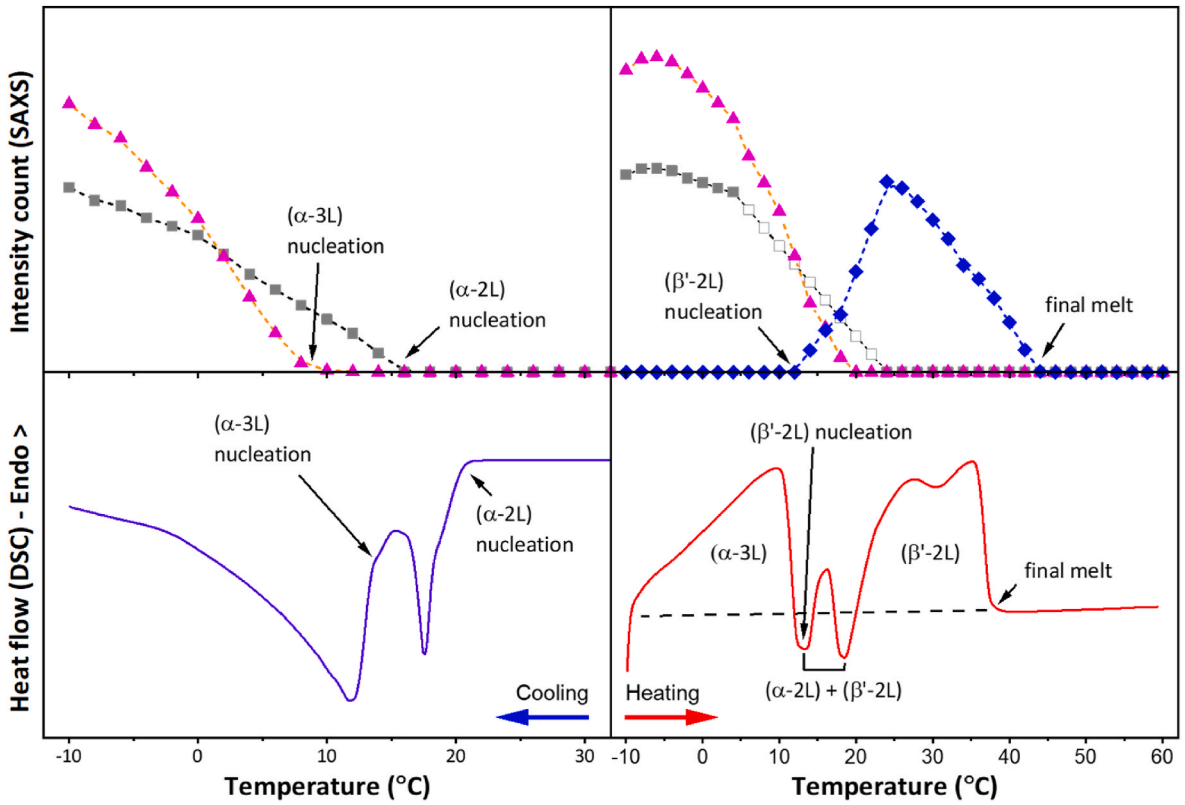

Fig. 5. Phase evolution pathway two: The β′-phase appears during heating treatment. For instance, the Mid fraction cooled from melt at −2 °C/min to −10 °C, followed by subsequent heating at 2 °C/min to 60 °C displays this pathway. Trends of the α-2L phase (gray line with square symbols) are shown together with the α-3L phase (magenta line with triangle symbols) and the β′-2L phase (blue line with diamond symbols). The hollow squares indicate estimated data points derived from the wide angle X-ray scattering data. (For interpretation of the references to colour in this figure legend, the reader is referred to the Web version of this article.)

about 13–15 °C. Therefore, some intensity data points (Fig. 5, hollow squares) were estimated from the trend of disappearance of the α-peak in the wide angle region ($q = 1.52$ Å^{-1}). It is likely that this transformation is melt-mediated, because the formation of the 2L-β′ phase occurs concomitantly to the melting of the α-crystals (Sato, 2018).

The DSC thermogram (Fig. 5, bottom panels) shows the three typical broad endothermic peaks of milk fat melting. By correlating these thermal events with the X-ray pattern evolution, we can associate the first peak to the melting of the α-3L crystals. The following minimum is an exothermic dip that is associated to the formation of the β′-2L crystals (see also the blue line in the SAXS panel of Fig. 5). Hence, the second thermal peak is probably the result of the α-2L melting and β′-2L nucleation. Finally, the last endothermic peak corresponds to the melting of the β′-2L structure. The current interpretation is in agreement with an *in-situ* DSC-SAXS study in cream crystallisation previously performed (Christelle Lopez, Bourgaux, Lesieur, Bernadou et al., 2002). Table 2 summarises the temperatures of the important thermal events for all samples at different cooling rates.

The last crystallisation pathway is only observed for the Stearin fraction at a cooling rate of −0.5 °C/min (Fig. 6). This pathway is different from the other more common two, because the formation of the β′-polymorph is observed during the cooling process rather than during subsequent heating stage. There are three nucleation events observable from the SAXS patterns: the first one at around 26 °C, corresponding to the α-2L crystal structure formation. However, this form is short-lived as observed from the decreasing in intensity of its characteristic wide angle peak at $q = 1.52$ Å^{-1}. Similarly to the heating process shown in Fig. 5, the decrease trend in X-ray intensities here are estimated from the characteristic WAXS peak intensity of the α-polymorph (hollow squares), due to the overlapping of the main α-2L and β′-2L peaks in the SAXS regime. The two following nucleation events at around 23 and 8 °C are associated with the formation of the β′-2L and β′-3L polymorphs, in this order.

Three nucleation events can also be observed from the thermograms, where three exothermic peaks are present with onsets at 27.0, 24.0 and 11.8 °C (Table 2). It is worth noting, that without the accompanying X-ray scattering data, these three exothermic events can be easily wrongly interpreted, especially when relying on the melting fractions concept (HMF, MMF, LMF). However, by combining both techniques we can be certain that a polymorphic transformation is taking place, indicated by the disappearing α-peak in the wide angle region. Moreover, the presence of two exothermic peaks during cooling ramp, related to the same 2L-stacking (α-2L and β′-2L), suggests that a polymorphic transformation has taken place from the α-2L to the β′-2L phase (Sato, 2018). This aligns with our previous interpretation that the α → β′ transformation occurs within the same stacking configuration in milk fat (Pratama et al., 2021).

Following the SAXS pattern in Fig. 6, no α-3L crystals were observed upon cooling as the 3L structure directly nucleated into a β′-phase. In contrast, at higher cooling rates of −2 and −5 °C/min (Fig. 5), Stearin also crystallised in the α-3L form. According to the Ostwald's rule of stages, TAGs normally nucleate into the less stable form (α-phase) given appropriate undercooling, which can be kinetically favoured, and then transform into a more stable polymorph (e.g., the β′-phase) (Himawan et al., 2006). However, the slow cooling rate of −0.5 °C/min provided low undercooling, which can override this rule (Himawan et al., 2006) and result in the direct nucleation of a more stable form (β′-3L in this case). It is worth noting that this same cooling rate did not produce β′-3L in other milk fat fraction samples (Fig. S2). We attribute this to the high amount of short-FA TAGs in the other samples, which hinder the α → β′ transformation.

In contrast to the second pathway, there are no polymorphic

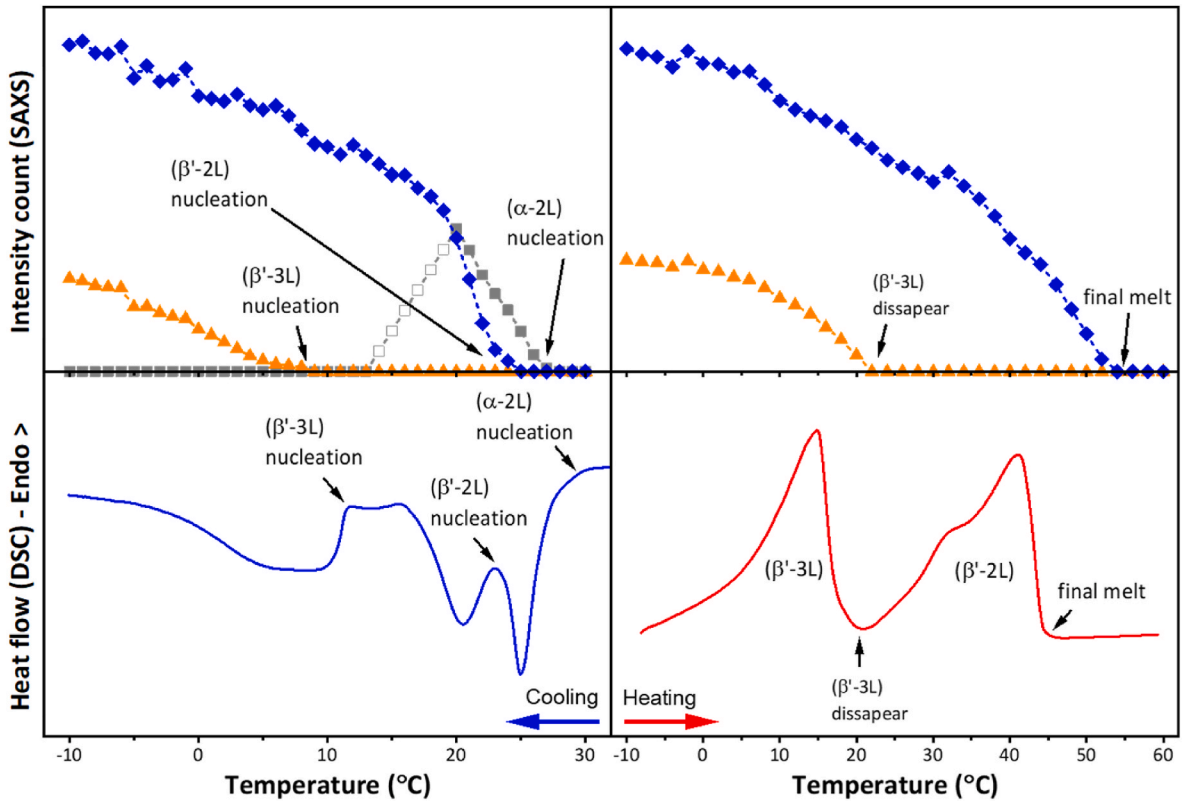

Fig. 6. Phase evolution pathway three: The β′-phase appears during cooling treatment. Only the Stearin fraction cooled from melt at −0.5 °C/min to −10 °C, followed by subsequent heating at 2 °C/min to 60 °C displays this pathway. Trends of the α-2L phase (gray line with square symbols) are shown together with the β′-3L phase (orange line with triangle symbols) and the β′-2L phase (blue line with diamond symbols). The hollow squares indicate estimated data points derived from the wide angle X-ray scattering data. (For interpretation of the references to colour in this figure legend, the reader is referred to the Web version of this article.)

transformation occurring during the subsequent heating stage (cp. Figs. 5 and 6). Instead, two separate DSC endothermic peaks are observable, which are linked to the melting of the two crystal forms of β′-3L and β′-2L. It is worth pointing out that the Stearin fraction cooled at −5 and −2 °C/min showed three melting peaks in its thermogram, whereas the −0.5 °C/min rate showed only two melting events. This provides further evidence that the thermal characteristics of milk fat are largely affected by the TAG composition as well as the processing conditions that precede the heating scan.

3.4. *Effect of the cooling rate on the thermal properties of different milk fat samples*

One of the objectives of testing the same heating rate of 2 °C/min for all samples was to evaluate if the different preceding cooling rates can affect the melting range of the different fractions. This depends on the type of polymorphs present, their crystallinity and the TAGs composition. As can be seen in Table 2, the melting range of the milk fat fractions are largely different. Stearin fraction have the highest, whereas Olein fraction display the lowest melting points among all samples. This trend can be easily understood as being the result of varying amounts of high melting TAGs (all-SFA). Furthermore, the effect of the cooling rate on the melting range was investigated. Whole Fat, Stearin and Mid fraction samples cooled at −0.5 °C/min showed about 0.6–1.1 °C higher final melting points (see notation on Figs. 4–6) than the same sample cooled at −5 °C/min. This trend is in accordance with our previous study on buffalo and cow milk fat (Pratama et al., 2021), where slow cooling resulted in higher melting points. Noting that the three samples display the β′-2L phase at the end of melting process, one can attribute the enhanced melting point as a result of (i) higher amount of β′-2L crystalline material formed during a slower cooling process and (ii) the difference in β′-2L crystal packing density as affected by the crystallisation time. Indeed, we previously observed a similar phenomenon with a pure milk fat asymmetrical TAG (1-butyryl 2-stearoyl 3-palmitoyl-glycerol), that a long isothermal hold allowed the β′-crystal packing to become more dense. As a consequence, the strength of Van der Waals interactions between hydrocarbon chains can increase and lead to a higher melting temperature (Pratama et al., 2022).

With a similar argument, we can also explain, why the melting point of the Olein fraction is not much affected by the cooling rate, with the −5 and −0.5 °C/min rates, giving the same final melting temperature of 17.1 °C. The Olein fraction did not form β′ crystals upon heating, and stayed in the hexagonal packing of the α-polymorph. We note that the chain packing in the α-form is characterised by the hydrocarbon chains undergoing free rotations along their long axis, and in turn not allowing the chain packing to become significantly denser with time, i.e., the Van der Waals interactions remain practically constant in this case. Hence, different crystallisation times (more or less time at high undercooling) do not have a significant effect on the melting temperatures.

Another interesting observation concerns the similar melting properties of the Mid fraction and the Whole Fat sample. Indeed, the Mid fraction is the result of the Whole Fat sample being separated from most of its ‘higher’ and ‘lower’ melting TAGs. One could think that, upon removal of the high melting TAGs, the Mid fraction would have a lower melting point. However, due to co-crystallisation and entrapment during fractionation, the Mid fraction has actually a TAG composition that is close to the original Whole Fat sample (Fig. 1), and thus sustains their similar thermal and melting properties.

3.5. *Microstructure of different milk fat fractions*

The microstructure of milk fat crystals is of interest as it influences

food quality attributes, such as mouthfeel. For instance, large crystal size has been associated with an unpleasant grainy texture in butter. Here, we report the microstructure of the milk fat fractions with different TAGs composition, as they are cooled from melt at −5 °C/min (Fig. 7). The amount of the high melting all-SFA in the sample played a significant role in the nucleation temperature, as can be seen in Table 2, where Stearin α-2L nucleated at higher temperatures than the Whole Fat and Mid fraction. Micrographs (Fig. 7) show that Stearin fraction samples nucleated at temperatures above 25 °C, whereas Whole Fat and Mid fraction samples presented their first nucleation events at about 20 °C. Lastly, the Olein fraction, which has the lowest all-SFA content nucleated only below 15 °C.

Supported by our SAXS and DSC findings, we are interested to deliver best interpretations of the PLM images. For instance, the two nucleation events, which correspond to the appearance of α-2L and α-3L crystals, are clearly observed in the Whole Fat and Mid fraction samples. The nucleation of the α-2L polymorph is evident, when large bright crystal clusters appeared at 20 °C, whereas the second nucleation event (α-3L) is observed from the appearance of smaller crystal agglomerates that filled out the molten sample at 15 °C, and grew brighter as the cooling proceeded. More α-2L crystal clusters can be observed in the Mid fraction than in the Whole Fat sample, which is linked to its higher amount of all-SFA that corresponds to the α-2L crystals (Table 2, Fig. 1). The second nucleation event in the Stearin fraction is harder to observe due to the high concentration of all-SFA TAGs that results in higher amount of α-2L nuclei. However, focusing on the area indicated by the yellow arrow (Fig. 7, second row), we can see the formation of new crystal nuclei at 15 °C. In contrast, only one nucleation event is visible in the Olein fraction, with the formation of streaky crystal clusters at 10 °C, corresponding to the α-3L polymorph. These microscopy evaluations are in accordance with the results obtained from SAXS and DSC measurements, despite differences in the measurement set ups affecting the exact temperature values of the crystallisation events.

One particular experiment of interest concerned the cooling of the Stearin fraction at −0.5 °C/min. In fact, this experiment did display three nucleation events (Fig. 6). Fig. 8 shows the microstructures formed upon slow cooling, and we can confirm three separate events also at the micro-scale level. The first nucleation event is observed at 29.5 °C, which corresponds to the appearance of α-2L crystals. The nuclei are less in number but grow bigger, compared to the −5 °C/min cooling rate (nucleation seen at 25 °C, Fig. 7). The same trend was observed in buffalo and cow whole milk fat upon slow and fast cooling (Pratama et al., 2021). The second nucleation event is visible with the appearance of a corona of small crystals surrounding the existing agglomerates, at about 20 °C. This structure corresponds to the formation of β′-2L crystals, recorded in DSC at 24.0 °C (Table 2). It is worth noting, that according to the SAXS measurements, the α-crystal intensity diminishes when the β′-2L nucleates (Fig. 6). However, the micrographs do not indicate that the initial nuclei of α-2L disappeared, when the corona was formed. A possible explanation is that the α-2L nuclei transform into β′-2L under solid state transformation, emphasizing the lack of melting of the metastable phase. This transformation type is contrasting to melt-mediated ones, where the α-2L melts before the formation of β′-2L phase during heating process (Fig. 5). Indeed, the continuous slow cooling process kept the temperature below the melting point of α-2L crystals, which in turn provides a suitable condition for this solid state polymorphic transition (Sato, 2018). However, PLM provides lower resolution compared to SAXS and DSC techniques, so that some nano-scale changes (for example, α-crystals melting and β′-crystals forming concomitantly) might not be visible. Finally, the third nucleation event can be seen with the formation of elongated crystal agglomerates, which appeared at about 10 °C. This event corresponds to the formation of the β′-3L polymorph, which was recorded at 11.8 °C in the DSC measurements (Table 2).

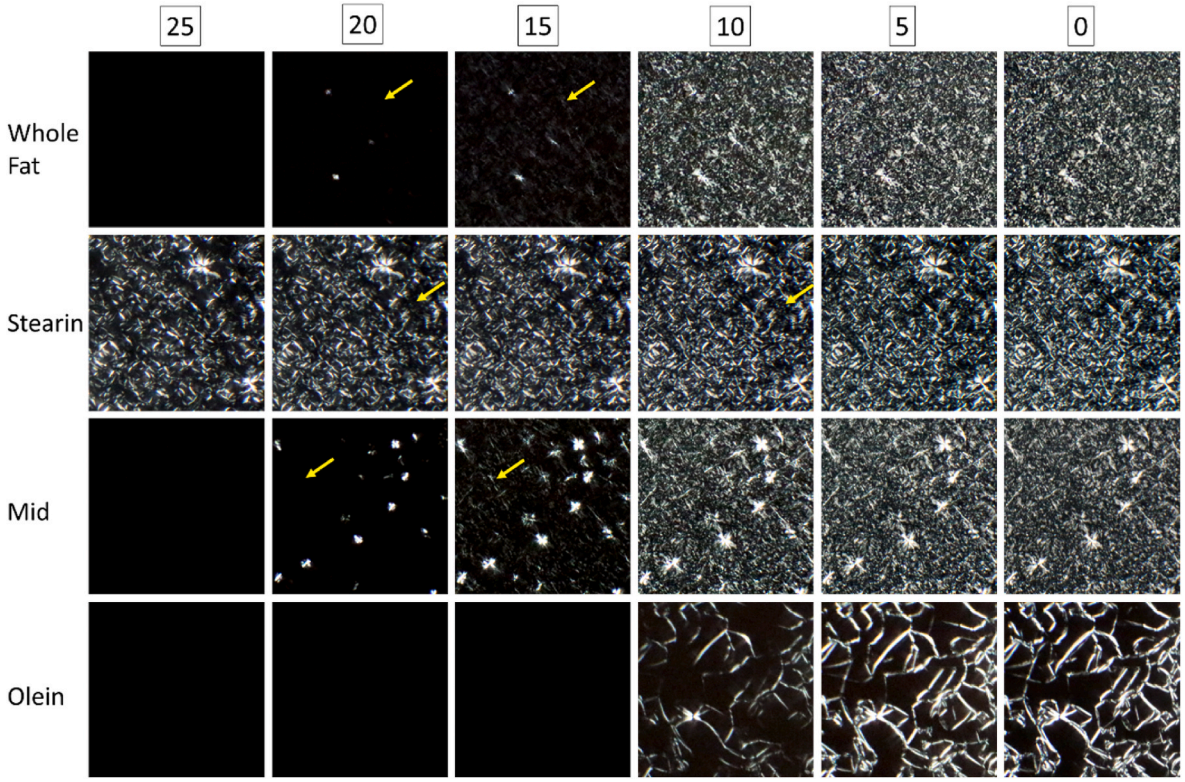

Fig. 7. Crystal microstructure of milk fat samples during the cooling scan from the melt at −5 °C/min. Captured images are presented from 25 to 0 °C at 5 °C interval. Each side corresponds to 200 μm. Yellow arrows indicate the formation of new crystals in the void (second nucleation). (For interpretation of the references to colour in this figure legend, the reader is referred to the Web version of this article.)

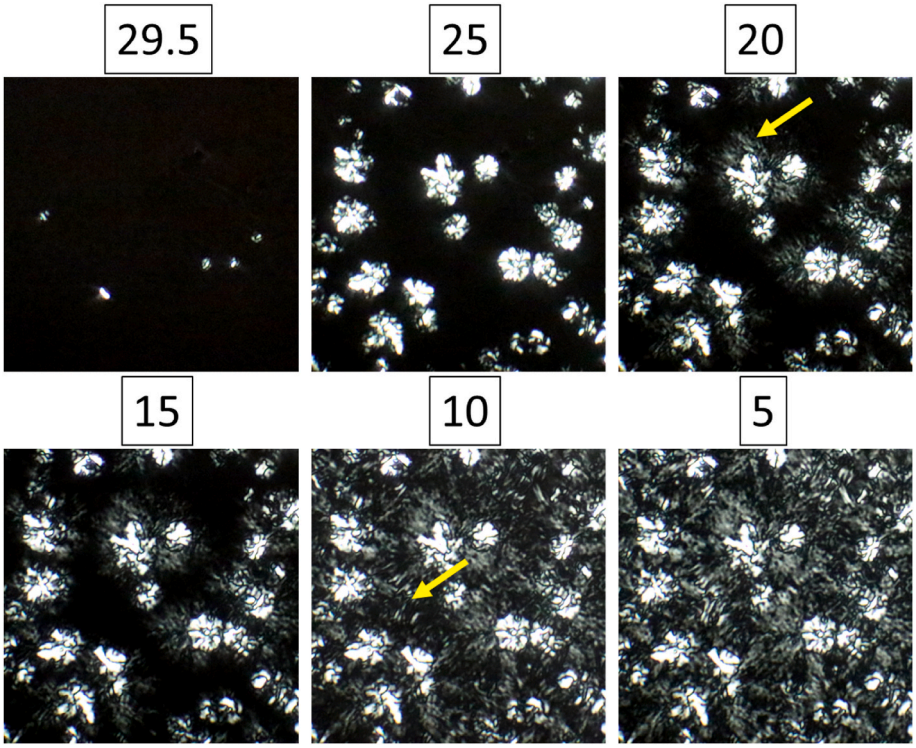

Fig. 8. Crystal microstructure formation in the Stearin fraction on cooling from melt at −0.5 °C/min. Captured images are presented from 25 to 0 °C at 5 °C interval. Each image side corresponds to 200 μm. Yellow arrows indicate the formation of new crystals in the void (second and third nucleation). (For interpretation of the references to colour in this figure legend, the reader is referred to the Web version of this article.)

4. Conclusion and outlook

We have shown that 2L-stacked crystals are formed mainly in fractions rich in all-SFA TAGs, whereas the 3L form is mainly related to the presence of single and multi-UFA TAGs. The short-FA TAGs are not easily incorporated in the solid crystals and are found in higher quantity in the liquid fraction. Furthermore, this type of TAGs does contribute to delayed polymorphic transformations. In this study, we once more confirmed the main contribution of each TAG groups to the different crystalline forms in milk fat, and discussed how they interact as a mixture in determining the crystallisation kinetics. Here, the TAGs composition or specifically the TAG groups ratios play a significant role in crystallisation. For instance, the Stearin fraction forms the β′-polymorph during slow cooling, due a relatively small proportion of short-FA TAGs that can impede the α to β′ phase transformation. The opposite effect applies to the Olein fraction, which is unable to form the β′ phase under the given experimental conditions, because of its higher content of short-FA TAGs. However, the crystallisation kinetics of the Whole Fat and Mid fraction samples behave very similarly despite some compositional differences. This suggests that in order to induce a significant change in the kinetics of polymorphic transformations, compositional differences need to be quite significant, as given in the Stearin and Olein fractions.

With respect to future TAGs composition design-focussed studies, Bayard et al. (2022) found that the addition of 1% tristearin had little effect to the nanostructure of milk fat crystals. In contradiction, our past study (Pratama et al., 2021) found that TAGs composition differences in buffalo and cow milk fat, albeit not as substantial as the Stearin and Olein fractions with respect to the Mid fraction or Whole Fat sample, are sufficient to induce a difference in the type and ratio of different polymorphs at the end of a slow cooling profile. Nonetheless, due to the complexity of milk fat TAGs, it is virtually impossible to mimic changes in its composition using a model system approach, as for cocoa butter with its three main TAGs only (Ghazani & Marangoni, 2021). The use of actual fat or fat fractions is thus the only practical option for fine-tuning the crystallisation behaviour of milk fat products. For this purpose, we argue that a robust and accurate compositional analysis technique is very important. To date many chromatographic studies published on the milk fat TAGs composition (Christelle Lopez, 2018; Christelle Lopez et al., 2006; Gresti et al., 1993; Zhou et al., 2014), reported as low as 17 (Wright et al., 2000) to more than 3000 (Liu et al., 2020) TAG species with varying concentration. This highly affects the interpretation of the obtained compositional results, especially regarding the TAG groups ratios. A better understanding of the interaction effects between all-SFA, single and multi-UFA as well as short-FA TAG groups will allow us to predict the possible crystallisation pathways and kinetics, and even further, to design compositional modification strategies in order to achieve specific milk fat crystallisation characteristics.

CRediT authorship contribution statement

Yoga Pratama: Funding acquisition, Conceptualization, Methodology, Investigation, Writing – original draft. **Julia Seilert:** Formal analysis, Writing – review & editing. **Amin Sadeghpour:** Writing – review & editing. **Elena Simone:** Funding acquisition, Writing – review & editing. **Michael Rappolt:** Supervision, Methodology, Resources, Writing – review & editing.

Declaration of competing interest

The authors declare that they have no known competing financial interests or personal relationships that could have appeared to influence the work reported in this paper.

Data availability

Data will be made available on request.

Acknowledgements

The authors are grateful for the funding provided by Indonesian Endowment Fund for Education (LPDP) in the form of full scholarship for Ph.D. study of Yoga Pratama. ES has received funding for this project from the European Research Council (ERC) under the European Union's Horizon 2020 research and innovation programme (grant agreement no. 949229).

Appendix A. Supplementary data

Supplementary data to this article can be found online at https://doi.org/10.1016/j.lwt.2023.115274.

References

Abd El-Salam, M. H., & El-Shibiny, S. (2011). A comprehensive review on the composition and properties of buffalo milk. *Dairy Science & Technology, 91*(6), 663–699. https://doi.org/10.1007/s13594-011-0029-2

Bayard, M., Kauffmann, B., Vauvre, J.-M., Leal-Calderon, F., & Cansell, M. (2022). Isothermal crystallization of anhydrous milk fat in presence of free fatty acids and their esters: From nanostructure to textural properties. *Food Chemistry, 366*(June 2021), Article 130533. https://doi.org/10.1016/j.foodchem.2021.130533

Breitschuh, B., & Windhab, E. J. (1998). Parameters influencing cocrystallization and polymorphism in milk fat. *Journal of the American Oil Chemists' Society 1998 75:8, 75*(8), 897–904. https://doi.org/10.1007/S11746-998-0264-8

Campos, R. J., Litwinenko, J. W., & Marangoni, A. G. (2003). Fractionation of milk fat by short-path distillation. *Journal of Dairy Science, 86*(3), 735–745. https://doi.org/10.3168/jds.S0022-0302(03)73654-6

Che Man, Y. B., Haryati, T., Ghazali, H. M., & Asbi, B. A. (1999). Composition and thermal profile of crude palm oil and its products. *Journal of the American Oil Chemists' Society, 76*(2), 237–242. https://doi.org/10.1007/s11746-999-0224-y

Cisneros, A., Mazzanti, G., Campos, R., & Marangoni, A. G. (2006). Polymorphic transformation in mixtures of high- and low-melting fractions of milk fat. *Journal of Agricultural and Food Chemistry, 54*(16), 6030–6033. https://doi.org/10.1021/jf0600814

Deffense, E. (1993). Milk fat fractionation today: A review. *Journal of the American Oil Chemists' Society, 70*(12), 1193–1201. https://doi.org/10.1007/BF02564225

Dimick, P. S., Reddy, S. Y., & Ziegler, G. R. (1996). Chemical and thermal characteristics of milk-fat fractions isolated by a melt crystallization. *Journal of the American Oil Chemists' Society, 73*(12), 1647–1652. https://doi.org/10.1007/BF02517966

FAO. (2022). FAOSTAT statistical database. https://www.fao.org/faostat/en/#data/QCL.

Gantner, V., Mijić, P., Baban, M., Škrtić, Z., & Turalija, A. (2015). The overall and fat composition of milk of various species. *Mljekarstvo, 65*(4), 223–231. https://doi.org/10.15567/mljekarstvo.2015.0401

Ghazani, S. M., & Marangoni, A. G. (2021). Molecular origins of polymorphism in cocoa butter. *Annual Review of Food Science and Technology, 12*, 567–590. https://doi.org/10.1146/annurev-food-070620-022551

Gresti, J., Bugaut, M., Maniongui, C., & Bezard, J. (1993). Composition of molecular species of triacylglycerols in bovine milk fat. *Journal of Dairy Science, 76*(7), 1850–1869. https://doi.org/10.3168/jds.S0022-0302(93)77518-9

Grotenhuis, E. T., Van Aken, G. A., Van Malssen, K. F., & Schenk, H. (1999). Polymorphism of milk fat studied by differential scanning calorimetry and real-time X-ray powder diffraction. *Journal of the American Oil Chemists' Society, 76*(9), 1031–1039. https://doi.org/10.1007/s11746-999-0201-5

Grummer, R. R. (1991). Effect of feed on the composition of milk fat. *Journal of Dairy Science, 74*(9), 3244–3257. https://doi.org/10.3168/JDS.S0022-0302(91)78510-X

Himawan, C., Starov, V. M., & Stapley, A. G. F. (2006). Thermodynamic and kinetic aspects of fat crystallization. *Advances in Colloid and Interface Science, 122*(1–3), 3–33. https://doi.org/10.1016/j.cis.2006.06.016. Elsevier.

Jensen, R. G., Ferris, A. M., & Lammi-Keefe, C. J. (1991). The composition of milk fat. *Journal of Dairy Science, 74*(9), 3228–3243.

Larsen, M. K., Andersen, K. K., Kaufmann, N., & Wiking, L. (2014). Seasonal variation in the composition and melting behavior of milk fat. *Journal of Dairy Science, 97*(8), 4703–4712. https://doi.org/10.3168/jds.2013-7858

Liu, Z., Li, C., Pryce, J., & Rochfort, S. (2020). Comprehensive characterization of bovine milk lipids: Triglycerides. *ACS Omega, 5*(21), 12573–12582. https://doi.org/10.1021/ACSOMEGA.0C01841

Loisel, C., Keller, G., Lecq, G., Bourgaux, C., & Ollivon, M. (1998). Phase transitions and polymorphism of cocoa butter. *Journal of the American Oil Chemists' Society, 75*(4), 425–439. https://doi.org/10.1007/s11746-998-0245-y

Lopez, C. (2018). Crystallization properties of milk fats. In K. Sato (Ed.), *Crystallization of lipids: Fundamentals and applications in food, cosmetics and pharmaceuticals* (pp. 283–321). Wiley Blackwell. https://doi.org/10.1002/9781118593882.ch10.

Lopez, C., Bourgaux, C., Lesieur, P., Bernadou, S., Keller, G., & Ollivon, M. (2002). Thermal and structural behavior of milk fat 3. Influence of cooling rate and droplet size on cream crystallization. *Journal of Colloid and Interface Science, 254*(1), 64–78. https://doi.org/10.1006/jcis.2002.8548

Lopez, C., Bourgaux, C., Lesieur, P., & Ollivon, M. (2002). Crystalline structures formed in cream and anhydrous milk fat at 4 °C. *Le Lait, 82*(3), 317–335. https://doi.org/10.1051/lait:2002013

Lopez, C., Bourgaux, C., Lesieur, P., Riaublanc, A., & Ollivon, M. (2006). Milk fat and primary fractions obtained by dry fractionation. 1. Chemical composition and crystallisation properties. *Chemistry and Physics of Lipids, 144*(1), 17–33. https://doi.org/10.1016/j.chemphyslip.2006.06.002

Lopez, C., Lavigne, F., Lesieur, P., Bourgaux, C., & Ollivon, M. (2001). Thermal and structural behavior of milk fat. 1. Unstable species of anhydrous milk fat. *Journal of Dairy Science, 84*(4), 756–766. https://doi.org/10.3168/jds.S0022-0302(01)74531-6

Lopez, C., Lesieur, P., Bourgaux, C., & Ollivon, M. (2005). Thermal and structural behavior of anhydrous milk fat. 3. Influence of cooling rate. *Journal of Dairy Science, 88*(2), 511–526. https://doi.org/10.3168/jds.S0022-0302(05)72713-2

MacRidachis, J., Bayés-García, L., & Calvet, T. (2021). Mixing phase behavior of tripalmitin and oleic-rich molecular compound-forming triacylglycerols. *Industrial & Engineering Chemistry Research, 60*(15), 5374–5384. https://doi.org/10.1021/acs.iecr.1c00324

Marangoni, A. G., & Lencki, R. W. (1998). Ternary phase behavior of milk fat fractions. *Journal of Agricultural and Food Chemistry, 46*(10), 3879–3884. https://doi.org/10.1021/jf9801668

Maurice-Van Eijndhoven, M. H. T., Hiemstra, S. J., & Calus, M. P. L. (2011). Short communication: Milk fat composition of 4 cattle breeds in The Netherlands. *Journal of Dairy Science, 94*(2), 1021–1025. https://doi.org/10.3168/JDS.2009-3018

Nguyen, V., Duong, C. T. M., & Vu, V. (2015). Effect of thermal treatment on physical properties and stability of whipping and whipped cream. *Journal of Food Engineering, 163*, 32–36. https://doi.org/10.1016/J.JFOODENG.2015.04.026

Omar, Z., Hishamuddin, E., Sahri, M. M., Fauzi, S. H. M., Dian, N. L. H. M., Ramli, M. R., & Rashid, N. A. (2015). Palm oil crystallisation: A review. *Journal of Oil Palm Research, 27*(2), 97–106.

Palmquist, D. L., Denise Beaulieu, A., & Barbano, D. M. (1993). Feed and animal factors influencing milk fat composition. *Journal of Dairy Science, 76*(6), 1753–1771. https://doi.org/10.3168/JDS.S0022-0302(93)77508-6

Pratama, Y., Burholt, S., Baker, D. L., Sadeghpour, A., Simone, E., & Rappolt, M. (2022). Polymorphism of a highly asymmetrical triacylglycerol in milk fat: 1-Butyryl 2-stearoyl 3-Palmitoyl-glycerol. *Crystal Growth & Design, 22*(10), 6120–6130. https://doi.org/10.1021/acs.cgd.2c00713

Pratama, Y., Simone, E., & Rappolt, M. (2021). The unique crystallization behavior of Buffalo milk fat. *Crystal Growth & Design, 21*(4), 2113–2127. https://doi.org/10.1021/acs.cgd.0c01543

Ramel, P. R., & Marangoni, A. G. (2016). Engineering the microstructure of milk fat by blending binary and ternary mixtures of its fractions. *RSC Advances, 6*(47), 41189–41194. https://doi.org/10.1039/c6ra07114g

Romano, R., Giordano, A., Chianese, L., Addeo, F., & Musso, S. S. (2011). Triacylglycerols, fatty acids and conjugated linoleic acids in Italian Mozzarella di Bufala Campana cheese. *Journal of Food Composition and Analysis, 24*(2), 244–249. https://doi.org/10.1016/J.JFCA.2010.10.004

Rønholt, S., Mortensen, K., & Knudsen, J. C. (2013). The effective factors on the structure of butter and other milk fat-based products. *Comprehensive Reviews in Food Science and Food Safety, 12*(5), 468–482. https://doi.org/10.1111/1541-4337.12022

Sato, K. (2018). Polymorphism of lipid crystals. In K. Sato (Ed.), *Crystallization of lipids: Fundamentals and applications in food, cosmetics and pharmaceuticals* (pp. 17–60). Wiley Blackwell. https://doi.org/10.1002/9781118593882.ch2.

Schmelzer, J. M., & Hartel, R. W. (2001). Interactions of milk fat and milk fat fractions with confectionery fats. *Journal of Dairy Science, 84*(2), 332–344. https://doi.org/10.3168/JDS.S0022-0302(01)74482-7

Shi, Y., Smith, C. M., & Hartel, R. W. (2001). Compositional effects on milk fat crystallization. *Journal of Dairy Science, 84*(11), 2392–2401. https://doi.org/10.3168/jds.S0022-0302(01)74688-7

Smiddy, M. A., Huppertz, T., & van Ruth, S. M. (2012). Triacylglycerol and melting profiles of milk fat from several species. *International Dairy Journal, 24*(2), 64–69. https://doi.org/10.1016/j.idairyj.2011.07.001

Soyeurt, H., Dardenne, P., Gillon, A., Croquet, C., Vanderick, S., Mayeres, P., Bertozzi, C., & Gengler, N. (2006). Variation in fatty acid contents of milk and milk fat within and across breeds. *Journal of Dairy Science, 89*(12), 4858–4865. https://doi.org/10.3168/JDS.S0022-0302(06)72534-6

Timms, R. E. (1980). The phase behaviour and polymorphism of milk fat, milf fat fractions and fully hardened milk fat. *Australian Journal of Dairy Technology, 35*, 47–52.

Tomaszewska-Gras, J. (2013). Melting and crystallization DSC profiles of milk fat depending on selected factors. *Journal of Thermal Analysis and Calorimetry, 113*(1), 199–208. https://doi.org/10.1007/S10973-013-3087-2/TABLES/3

Tzompa-Sosa, D. A., Meurs, P. P., & van Valenberg, H. J. F. (2018). Triacylglycerol profile of summer and winter bovine milk fat and the feasibility of triacylglycerol fragmentation. *European Journal of Lipid Science and Technology, 120*(3), Article 1700291. https://doi.org/10.1002/ejlt.201700291

Van Aken, C. A., Ten Grotenhuis, E., Van Langevelde, A. J., & Schenk, H. (1999). Composition and crystallization of milk fat fractions. *Journal of the American Oil Chemists' Society, 76*(11), 1323–1331. https://doi.org/10.1007/s11746-999-0146-8

Wright, A. J., McGauley, S. E., Narine, S. S., Willis, W. M., Lencki, R. W., & Marangoni, A. G. (2000). Solvent effects on the crystallization behavior of milk fat fractions. *Journal of Agricultural and Food Chemistry, 48*(4), 1033–1040. https://doi.org/10.1021/jf9908244

Yao, Y., Liu, W., Zhang, D., Li, R., Zhou, H., Li, C., & Wang, S. (2020). Dynamic changes in the triacylglycerol composition and crystallization behavior of cocoa butter.

Lebensmittel-Wissenschaft und -Technologie, 129, Article 109490. https://doi.org/10.1016/j.lwt.2020.109490

Zeb, A., & Murkovic, M. (2010). Analysis of triacylglycerols in refined edible oils by isocratic HPLC-ESI-MS. *European Journal of Lipid Science and Technology, 112*, 844–851. https://doi.org/10.1002/ejlt.201000064

Zhou, Q., Gao, B., Zhang, X., Xu, Y., Shi, H., & Yu, L. (2014). Chemical profiling of triacylglycerols and diacylglycerols in cow milk fat by ultra-performance convergence chromatography combined with a quadrupole time-of-flight mass spectrometry. *Food Chemistry, 143*, 199–204. https://doi.org/10.1016/j.foodchem.2013.07.114